A mathematical model for assessing transient airborne infection risks in a multi-zone hospital ward

Alexander J. Edwards [a,*], Lee Benson [b,c], Zeyu Guo [c], Martín López-García [d], Catherine J. Noakes [c], Daniel Peckham [e,f], Marco-Felipe King [c]

[a] *Centre for Doctoral Training in Fluid Dynamics, University of Leeds, Leeds, UK*
[b] *Biomathematics & Statistics Scotland (BioSS), Scotland, UK*
[c] *School of Civil Engineering, University of Leeds, Leeds, UK*
[d] *School of Mathematics, University of Leeds, Leeds, UK*
[e] *School of Medicine, University of Leeds, Leeds, UK*
[f] *Leeds Teaching Hospitals NHS Trust, Leeds, UK*

ARTICLE INFO

ABSTRACT

Quantification of the parameters influencing airborne infection risks associated with indoor activities in different settings can help in understanding outbreak dynamics and the effective implementation of mitigation strategies. This is particularly important in hospitals, where the consequence of infections amongst vulnerable individuals can be significant. Despite the transient occupancy and inter-connected nature of hospital wards, the majority of airborne risk models assume steady-state conditions and well-mixed air in a single zone. We propose a multi-zone model with both a fixed and time-varying infectious person. We use an adapted version of the Wells–Riley model to estimate transient airborne virus concentration, and account for time-varying behaviour in the indoor setting. Through a coupling with a CONTAM airflow network model, we incorporate the effects of ventilation patterns on inter-zonal flow rates to represent likely airflow in a realistic hospital ward. We use this approach to explore the difference in predictions from transient versus steady-state models across several scenarios. Results suggest that a steady-state approach could lead to an overestimation of infection risk or underestimation of quanta emission, especially when the infectious person is only present for a short period of time. The difference between models is most apparent in poorly ventilated spaces, illustrating how risks can build over time when infectious occupant movement is more frequent than the removal rate due to ventilation. The model highlights the importance of considering transient factors when assessing infection risks to ensure that the most effective mitigation strategies are implemented to address long and short timescale risks.

1. Introduction

Airborne transmission is an infection route for many pathogens such as Tuberculosis (TB), Influenza and more recently SARS-CoV-2 [1]. The COVID-19 pandemic has highlighted the importance of understanding the factors which influence airborne transmission and how we manage the associated risk. With respiratory diseases already being a major contributor to pressure on hospital systems such as the National Health Service (NHS) in the UK, even more so during the winter [2], it is especially important to minimise the transmission of nosocomial infections through the airborne route. Small exhaled respiratory aerosols, which rapidly evaporate to be typically less than 10 μm [3], can carry viral or bacterial particles through the air and then be inhaled by another individual with the risk of causing an infection. Larger aerosols emitted in a cough or sneeze can travel as far as 7–8 m [3,4], while the smallest ones can remain airborne for several hours, depending on their eventual size after desiccation, and their trajectories are determined by the surrounding airflow or behaviour. Understanding the transport of pathogens in the air and the influence of the ward layout and ventilation system is a crucial part of designing and managing hospital environments to mitigate airborne transmission risks.

Real world hospital environments are complex and busy spaces with a considerable level of transient activity including behaviour of health care workers (HCWs) and visitors entering, leaving and moving around the space. The concentration of airborne pathogens is also transient in nature and may depend on the emission rate from an

infected person [5] and governing airflow factors including ventilation within rooms and airflow between rooms. Particles may deposit out of the air over time on to surfaces, particularly in close proximity to a source [6,7] or may decay in infectiousness [8]. These factors must be considered in an appropriate way for the specific scenario in order to evaluate the concentration of pathogen in indoor spaces and thus, provide a better estimation of the epidemiological dynamics. However, many previous and current indoor transport and dispersion models only consider steady state behaviour, both spatially and temporally, whether this be through computational fluid dynamics (CFD) analysis [9–11] or risk assessments using the Wells–Riley model [9,12,13].

The Wells–Riley model [14,15] is widely used to estimate the influence of ventilation on the number of newly infected individuals during the time interval $[0, t]$ in an indoor setting, and is given by:

$$N(t) = S(1 - e^{\frac{-Ipqt}{Q}}),\qquad(1)$$

Here S is the number of susceptible individuals, I is the number of initially infectious individuals, p [m^3 min^{-1}] is the pulmonary rate of individuals, q [quanta min^{-1}] is the infectious quanta production rate and Q [m^3 min^{-1}] is the extract ventilation rate. The model aims to provide an assessment of the risk of infection for a given single zone, for a particular emission rate of infectious doses expressed through q [quanta min^{-1}]. A quantum is defined as the infectious airborne dose required to infect an individual with probability $1 - e^{-1}$ (≈ 0.632) [14].

Despite its ubiquity throughout the literature, the Wells–Riley model has some limitations [16] such as assuming well-mixed air within the space, assuming steady-state airflow and the use of quanta which is often back-calculated from steady-state models of outbreaks [17]. It is widely recognised that the use of quanta to describe infectious dose emitted is a simplification of the transmission process. Some studies have looked to relate this directly to emitted virus either through measurement [18] or through calculation [5], and a recent analysis has shown that quanta emission rates for different diseases can have very large ranges [19]. However, quanta based steady-state models have been shown to compare well to COVID-19 super-spreading outbreaks suggesting that the approach can be valuable for assessing risk [20]. The use of the concept of re-breathed air fraction [21] can take out the need for explicitly quantifying the ventilation rate within the model and this approach has been used to make time-averaged predictions based on measured CO_2 data [18,22]. Other studies have applied integrated spatial flow fractions [23] and the use of multi-zone models [17,24] which allow for the space to be sectioned into multiple zones which allows for varying behaviours, parameters and inter-zonal flows linking the space. However, these previous multi-zone models have used idealised airflow assumptions with steady-state quanta concentrations to demonstrate model behaviour rather than consider the ventilation in a realistic environment.

A better approximation of indoor airflow can be modelled using ventilation network models. CONTAM is one such model which allows for the simulation of airflow inside multi-zonal spaces and can model transient occupant and ventilation schedules, weather and wind effects such as wind pressure, wind speed, wind direction, relative humidity and external temperatures [25], and contaminant sources and ambient air pollutants, which may play a role in prolonging recovery for COVID-19 patients [26]. CONTAM is rarely used to provide Quantitative Microbial Risk Assessment (QMRA), but Yan et al. [27] illustrates the use of CONTAM for estimating airborne transmission of infectious pathogens in terms of quanta, for a multi-zone indoor setting through a coupling with the Wells–Riley model. Other studies such as those presented in Cheong et al. [28] and Shrestha et al. [29] use CONTAM to focus on the airflow, and how the implementation of mitigation strategies, such as ventilation, affects contaminant transport and infection risk. Parker et al. [30] uses CONTAM for airflow simulations, which are then coupled to a state-space approach when assessing risk of pollutant exposure in a multi-zone environment.

In this work, an adaptation of the Wells–Riley model is used to develop a transient multi-zonal approach to model the concentration of pathogen in the air and infection risk in a hospital scenario. The focus of the model is to explore short time duration effects (over a few hours). We evaluate how using a transient solution for the multi-zone system for concentration of pathogen in the air differs from the steady-state assumptions and the implications for predicting infection risks. This is illustrated through two case studies: (1) a scenario with a fixed patient infector who is stationary in one of the ward zones and (2) a scenario with a transient infector, representing an infectious healthcare worker (HCW) completing a drug round. The first scenario uses an idealised ventilation assumption to compare to Noakes and Sleigh [17] and López-García et al. [24]. The second transient infector case assumes that the infectious person moves from one zone to another in time within a geometry based on a UK respiratory ward, with transient inter-zonal flow values extracted from a CONTAM airflow simulation.

2. Methodology

2.1. Transmission model

Modelling transmission and outbreak dynamics is traditionally based on the Susceptible–Infected–Recovered (SIR) model, originally introduced by Kermack and McKendrick [31]. There have been many variations of this compartmental model, for example SIS assumes no immunity on recovery [24,32] and SEIR includes an incubation period [33]. These models have also been coupled to the Wells–Riley [12,24] to explore the impact of indoor conditions on outbreak dynamics. These epidemic models are suited to population scale simulations with a duration of several days or weeks, however in indoor settings such as a hospital ward, the complexity of interactions between people and admission-discharge patterns makes modelling the whole outbreak challenging.

Here, we consider a Susceptible–Exposed (SE) model where one considers the transmission dynamics in an indoor setting during a time interval $[0, T]$. In this time interval, $[0, T]$, we assume that newly infected individuals are taken to be exposed and infected but are not yet infectious due to being in the incubation period. This allows for a simplified compartmental model without the added complexity of new infections or accounting for changes in the population in the setting, allowing for focus purely on the model dynamics in the early stages. The equations used are:

$$\frac{dS(t)}{dt} = -\lambda S(t),$$
$$\frac{dE(t)}{dt} = \lambda S(t),\qquad(2)$$

where $S(t)$ represents the number of susceptible individuals at time t, and $E(t)$ the number of exposed (i.e. infected but not infectious) individuals at time t. The infection rate λ contains the parameter defining the number of infectious individuals in the indoor setting, $I(t) = I$, which is assumed to be constant during the time interval of interest $[0, T]$. To model transient effects the infection rate is considered to be time-dependent, and given by $\lambda(t) = pC(t)$, where p [m^3 min^{-1}] is the pulmonary rate and $C(t)$ [quanta m^{-3}] is the concentration of airborne pathogen at time t, which is characterised by the transport equation:

$$v\frac{dC(t)}{dt} = qI - QC(t).\qquad(3)$$

Here v [m^3] is the volume of the indoor space, q [quanta m^{-3}] is the infectious quanta production rate, Q [m^3 min^{-1}] is the ventilation rate and I is the number of infectious individuals, which all remain constant within the indoor space.

The standard Wells–Riley methodology defines a constant infection rate $\lambda = pC^*$, where $C^* = \frac{qI}{Q}$ is the steady state solution of Eq. (3).

On the other hand, a transient version involves defining $\lambda(t) = pC(t)$, where $C(t)$ is the actual transient solution of Eq. (3).

Following the approach in López-García et al. [24], the single-zone model can be extended to a transient multi-zone case for M zones:

$$v_k \frac{dC_k(t)}{dt} = q_k I_k - Q_k C_k(t) - \sum_{j=1}^{M} \beta_{kj} C_k(t) + \sum_{j=1}^{M} \beta_{jk} C_j(t), \quad k = 1, \ldots, M \quad (4)$$

where $C_k(t)$ is the quanta concentration in the air in zone k, I_k is the number of infectious individuals in zone k, Q_k [m³ min⁻¹] represents the extract ventilation rate in zone k, and q_k [quanta m⁻³] represents the quanta production rate in zone k. β_{kj} [m³ min⁻¹] are the inter-zonal flow rates between the zones, which is only non-zero if zone k is connected to zone j [24]. The individual zones represent single spaces such as rooms, bays, or corridors which are connected to other zones to form a multi-zone environment via doors. Larger rooms may also be split up into multiple zones themselves, which are connected directly through an opening from floor-to-ceiling and wall-to-wall. Multiple connected single zones form a multi-zone geometry.

In addition to Eq. (4), it is also necessary to extend the SE model presented in Eq. (2) for a multi-zone case, of M zones:

$$\frac{dS_k(t)}{dt} = -\lambda_k S_k(t),$$
$$\frac{dE_k(t)}{dt} = \lambda_k S_k(t),$$
$$\quad (5)$$

for $k = 1, \ldots, M$, where the infection rate becomes $\lambda_k = p_k C_k(t)$.

The system of equations given by Eq. (4), which models the concentration of pathogen in the air in each zone $k = 1, \ldots, M$, can be written in matrix form as

$$\mathbf{v} \frac{d\mathbf{C(t)}}{dt} = \mathbf{q} \circ \mathbf{I} - \mathbf{VC(t)} \quad (6)$$

where $\mathbf{C(t)}$ is the column vector of concentrations in each zone, which is spatially constant for any given time, inside a given zone. $\mathbf{V}$ is the ventilation matrix, $\mathbf{v}$ is the column vector of volumes for each zone, $\mathbf{q}$ is the column vector of quanta production rate for each zone and $\mathbf{I}$ is the column vector for the number of infectious individuals for each zone where the symbol $\circ$ represents the element-wise product of the two column vectors. This gives the ventilation matrix $\mathbf{V}$ as:

$$\mathbf{V} = \begin{pmatrix} Q_1 + \sum_k \beta_{1k} & -\beta_{21} & -\beta_{31} & \cdots & -\beta_{M1} \\ -\beta_{12} & Q_2 + \sum_k \beta_{2k} & -\beta_{32} & \cdots & -\beta_{M2} \\ -\beta_{13} & -\beta_{23} & \ddots & \ddots & -\beta_{M3} \\ \vdots & \vdots & \vdots & \vdots & \vdots \\ -\beta_{1M} & -\beta_{2M} & \cdots & -\beta_{M-1,M} & Q_M + \sum_k \beta_{Mk} \end{pmatrix}. \quad (7)$$

The inter-zonal flow rates, β_{kj} [m³ min⁻¹], can be approximated, informed by experiments, or extracted from other airflow simulations. In Case Study 1 (Section 3.1), constant and idealised values were used for both ventilation rates and inter-zonal flow rates for the whole simulation time. These were followed by models where the CONTAM software was used to determine the values of β_{kj} for a naturally ventilated hospital (Case Study 2 in Section 3.2). The theoretical details of the CONTAM model and the way in which the inter-zonal flow values are extracted can be seen in Section 2.2.

In a similar way, the steady-state system of zonal concentration of airborne pathogen can be recovered from Eq. (6) to give:

$$\mathbf{C}^* = \mathbf{V}^{-1} \mathbf{q} \circ \mathbf{I}. \quad (8)$$

which will be used as a comparison to the transient solution, obtained from numerically solving Eq. (6), in Sections 3.1 and 3.2.

It is worth noting that the Equations for concentration of pathogen in the air (Eqs. (3), (4) and (6)) do not include a turbulence flux term. This study aims to model long-range exposure across multi-connected zones rather than focus on short-range exposure, where turbulence fluxes would dominate. To evaluate short range exposures alternative approaches such as CFD modelling [7] or analytical approximation of aerosol size distributions with distance [34] would be needed.

2.2. Airflow simulations

CONTAM 3.4.0.3 [25,35] is used alongside the transmission model, described in Section 2.1, to determine inter-zonal flow values β_{kj}, used within the transmission model in Case Study 2 (Section 3.2). This allows for additional added complexity to the model allowing simulation of a naturally ventilated multi-zonal scenario, incorporating transient behaviour and weather effects. To extract the inter-zonal flow rates, the results of each simulation are processed using the CONTAM *Results Export Tool* [36,37]. This allows for the export of the airflow through each airflow element, which can then be used as the values for β_{kj} in Eq. (4), demonstrating the successful coupling of the two separate approaches.

We consider a multi-zonal hospital ward, where each zone is set to have an ambient temperature of $20°C$. For each zone k, we consider the air mass balance equation

$$[\sum_j m_{k,j} - \sum_j m_{j,k}] + m_{0,k} - m_{k,0} + m_{v,k} - m_{v,k} = 0, \quad (9)$$

where $m_{k,j}$ [kg min⁻¹] is the mass airflow entering zone j from zone k, and $m_{j,k}$ [kg min⁻¹] is the mass airflow entering zone k from zone j. $m_{0,k}$ [kg min⁻¹] is the total mass airflow entering zone k from the outside environment (e.g. leaks or natural ventilation such as windows) and $m_{k,0}$ [kg min⁻¹] is the total mass airflow leaving zone k into the outside environment. These can include through means of openings, leaks, doors and windows. $m_{k,v}$ [kg min⁻¹] is the total mass airflow extracted from zone k due to mechanical extract ventilation and $m_{v,k}$ [kg min⁻¹] is the total mass airflow for the mechanical supply ventilation to zone k.

In this case, we can link the inter-zonal flow rates in Section 2.1, with those above extracted from the CONTAM model, as

$$\beta_{kj} = \frac{m_{k,j}}{\rho_k}, \quad (10)$$

where ρ_k [kg m⁻³] is the air density in zone k.

When modelling windows, doors and other openings it is necessary to consider airflow rates through the opening as well as through gaps or leakage. In this case, the mass flow rate is calculated from the pressures using an orifice assumption through the power-law equation [38]

$$m_{k,j} = \rho_k C_{k,j} \Delta P_{k,j}^n. \quad (11)$$

Here ρ_k [kg m⁻³] is the air density in zone k, $C_{k,j}$ [m³ min⁻¹ Pa⁻ⁿ] is the discharge coefficient, $\Delta P_{k,j}^n$ [Paⁿ] is the pressure difference between zones k and j with n as the flow exponent.

Throughout the simulations in Section 3.2, the air leakage coefficient is set to be the default value, $C_{k,j} = 46.8$ m³ min⁻¹ Pa⁻ⁿ (equivalent to $C_{k,j} = 0.78$ m³ s⁻¹ Pa⁻ⁿ, as default in CONTAM). The flow exponent is also kept at the default value for CONTAM, $n = 0.5$. Flow exponents vary from $n = 0.5$ for large openings, where the flow is dominated by dynamic effects, to $n = 1$ for narrow openings dominated by viscous effects. [35].

The pressure in each zone is calculated based on the differences in air densities. This accounts for any temperature differences and consequent stack effects, based on the hydrostatic equation. Additionally, this requires the input of external pressures acting on the walls which is linked to the wind conditions as follows [38]:

$$P_{v,k} = \frac{1}{2} \rho_0 C_{P,k} v^2. \quad (12)$$

Where $P_{v,k}$ [kg m⁻¹ min⁻²] is the wind pressure on the external wall in question of zone k, ρ_0 [kg m⁻³] is the external air density, $C_{P,k}$ is the pressure coefficient at a leakage point and v [m min⁻¹] is the velocity of the wind at the given altitude.

In Section 3.2, a leakage flow path was modelled alongside each external window and each internal door using Eq. (11). We consider that doors between zones remained closed throughout, apart from when they were open for a 1 minute period to simulate the transient infectious HCW moving in and out of that particular zone. Windows remained closed for the full duration of the numerical simulation.
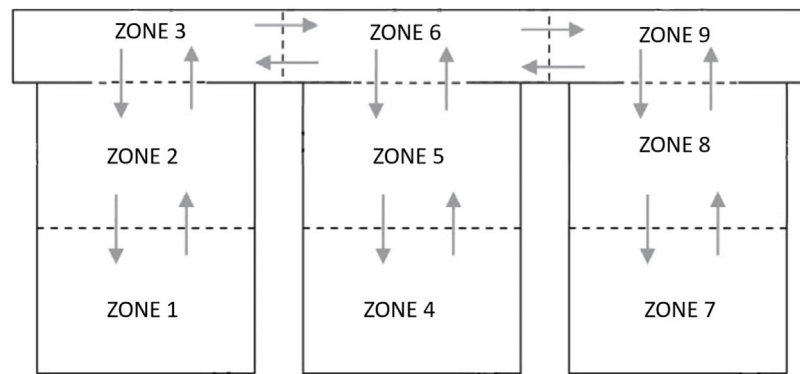
Fig. 1. Image showing the geometric set-up for the 9-zone ward set-up based on the set-up provided in López-García et al. [24] with each labelled zone.

3. Results and discussion

In this section, we present two case studies where we apply the methodology introduced in Section 2. These two scenarios aim to explore the influence of both an infector in a fixed location (an infectious patient), and a transient infector, representing, for example, an infectious HCW who completes a drug round.

3.1. Case study 1: Bed-bound infectious patient

3.1.1. The 9-zone hospital ward

To explore the case with a fixed infector who becomes infectious (or is admitted whilst being infectious) at $t = 0$ at a single location, the same idealised hospital ward scenario was used as in Noakes and Sleigh [17]. The geometry shown in Fig. 1 consists of 3 bays, each split up into two zones and an adjoining corridor which is split up into 3 zones, connecting the end of each bay.

The model assumes a steady-state ventilation scenario with the same amount of air supplied to and extracted from each zone (Setting A in Noakes and Sleigh [17]). Airflow between adjacent zones k and j is represented by an inter-zonal flow rate of $\beta_{k,j} = 9\,\mathrm{m^3\,min^{-1}}$. The supply and extract ventilation in each zone is $Q_k = 3\,\mathrm{m^3\,min^{-1}}$, $\forall k$, which leads to an overall ventilation rate of $27\,\mathrm{m^3\,min^{-1}}$. The volume of each zone is $v_k = 60\,\mathrm{m^3}$ $\forall k$ leading to a total ward volume of $v = 540\,\mathrm{m^3}$ and a total ventilation rate over the whole ward of 3 Air changes per hour (ACH). The inter-zonal flow set-up gives a case of homogeneous mixing in each zone i.e the net boundary flow is zero. It is assumed that there are 3 individuals in each zone, with the infector located in Zone 1, giving $S_0 = (2, 3, 3, 3, 3, 3, 3, 3, 3)$, $E_0 = 0$ for each zone, and $I_0 = 1$ in Zone 1 only, and is zero for all other zones. The quanta emission rate of the infector is taken to be $q_1 = 0.5$ quanta $\mathrm{min^{-1}}$ [17]. The pulmonary rate of all individuals is taken to be $p_k = 0.01\,\mathrm{m^3\,min^{-1}}$, $\forall k$. The total population is 27 individuals, leaving 26 susceptibles when accounting for the infectious person in Zone 1. The initial concentration is taken to be $C_0 = 0$ in each zone.

Eqs. (5) and (6) were solved over a time period of $< 8\,\mathrm{h}$ meaning that it is reasonable to assume that the occupancy does not change and that this is within the incubation period of the individuals who become exposed i.e there are no new infectious individuals.

3.1.2. Effect of ventilation rate

Fig. 2(c) shows the solution to the transient system (Eq. (6)) for concentration of airborne quanta at 3 ACH (as used in Noakes and Sleigh [17]) for each zone. This is plotted together with the steady-state (Eq. (8)) concentration of pathogen in the air (dashed lines) in each zone. The results show that there is a substantial difference between the steady-state solution and transient solution within the first hour. When using the steady-state model, as commonly used within the Wells–Riley model [14,15], there is an overestimation of the likely concentration,

which is due to the time taken for the concentration to build up in the space. For example, the infectious person is fixed in Zone 1, however for the steady-state assumption at time $t = 0$ in Zone 2, the concentration level is non-zero and is in fact, over half of the value of the zone where the infectious person is present. This is clearly unrealistic and is better approximated by the transient solution, as it takes a non-negligible amount of time for the concentration of pathogen to flow into the adjoining Zone 2 from Zone 1 and begin to increase.

The solutions for the quanta concentration with two lower ventilation rates are plotted in Figs. 2(b) and 2(a), where the extract ventilation is changed to $Q_k = 1.5\,\mathrm{m^3\,min^{-1}}$ and $Q_k = 0.5\,\mathrm{m^3\,min^{-1}}$, equating to 1.5 ACH and 0.5 ACH, respectively. As expected, as the ventilation rate in the space reduces, the overestimation in the steady-state model becomes more significant. In Fig. 2(a) the simulation was extended to 8 h to illustrate that the transient concentration solution does not reach steady-state until close to $7 - 8\,\mathrm{h}$ which is considerably longer than in the initial case of 3 ACH and even the case of 1.5 ACH. In addition to the effects on the accuracy of the model used, the change in ventilation rate also affects the absolute value of the transient and steady-state concentration of quanta in the space. For example, in the case of 3 ACH, even though the steady-state is reached significantly faster than for lower ACH, the predicted steady-state quanta concentration is much lower, illustrating the positive effect of ventilation on the mean concentration of quanta.

A fourth case with $Q_k = 6\,\mathrm{m^3\,min^{-1}}$ equating to 6 ACH is also presented in Fig. 2(d), showing the transient quanta concentration solution. This case was included as 6 ACH is the recommended ventilation rate in UK NHS hospital wards [39]. At 6 ACH, the transient model reaches the steady-state value in around 30 min, considerably faster than in the other cases. This would further increase in specialist environments such as intensive care wards where ventilation rates of 10 ACH are typically recommended. Although in reality many hospital wards do not reach the recommended standard, particularly where they are naturally ventilated, the results here suggests that should hospital wards be ventilated at 6 ACH, the transient effects become less significant and the steady-state model gives a reasonable approximation.

To illustrate this difference further, if we consider the first 30 min of an outbreak on a hospital ward, which is sufficiently prior to the stage at which any of the ventilation scenarios reach the steady-state value, then we can compare the relative difference between the transient concentration solution and that of the steady-state; this is shown in Fig. 3, illustrating the relative difference between the steady-state solution for concentration of pathogen compared to the transient solution, for 3 different zones plotted against increasing ventilation rate.

The results in Fig. 3 show that how appropriate the steady-state model is depends on both the ventilation rate and the zone. The higher the ventilation rate, the smaller the difference is between the two models and so the better the steady-state approximation becomes. However, a significant overestimation is evident in some zones. The
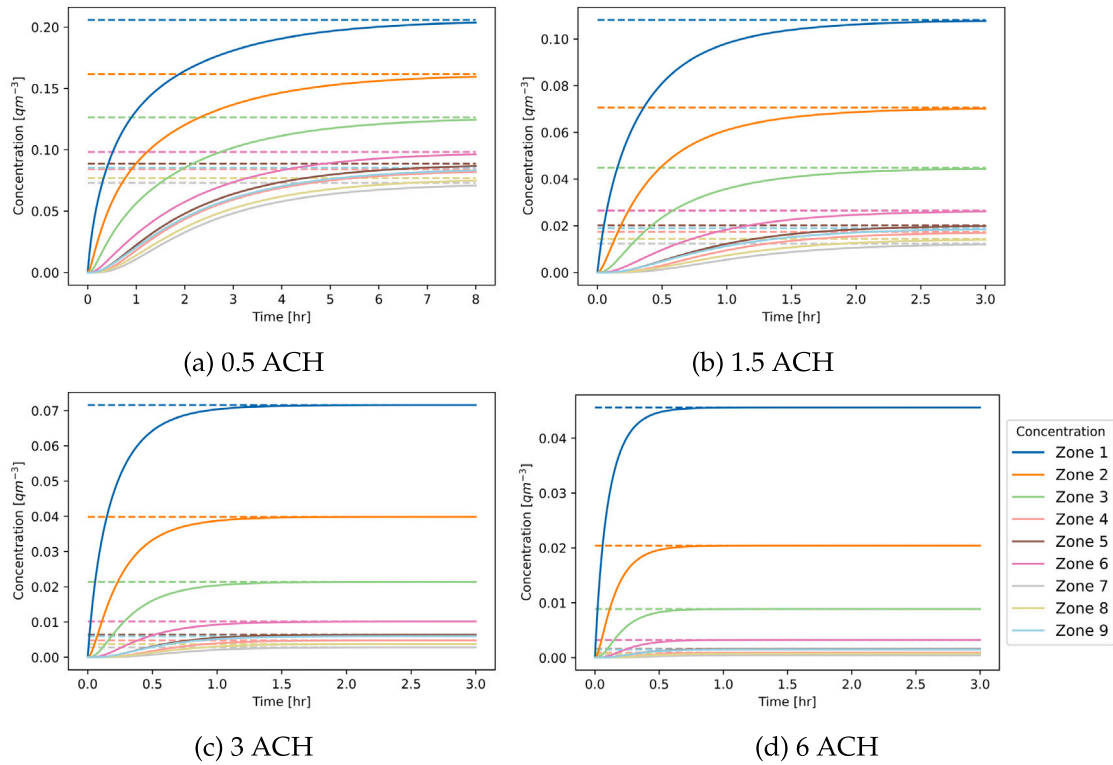
Fig. 2. The solution for the concentration of pathogen in the air with the transient solution (solid) and the steady-state solution (dashed) for various ventilation rates for the fixed infector case.
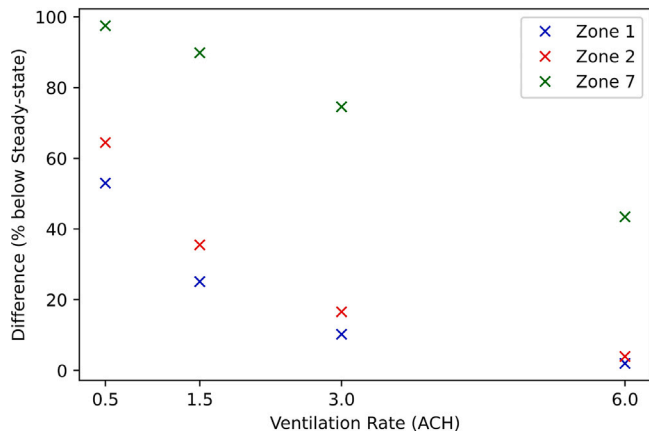

Fig. 3. The relative difference between the concentration values of the steady-state and the transient solution, calculated as $\frac{C^* - C(t=30\,\text{min})}{C^*}$ x 100, for Zone 1 (zone with Infector present), Zone 2 (zone adjacent to the Infector), and Zone 7 (zone furthest from the Infector) with 4 different ventilation settings for the fixed infector case.

steady-state approximation is closest to the transient model when the infectious individual is present in the same space. At 3 ACH, Zone 7, which is furthest from the infected individual is overestimated by almost 80% using a steady-state model, compared to less than 10% difference in Zone 1. At 6 ACH, we can see that although the transient effects are less important close to the infectious individual (i.e in Zone 1 or 2), as we move further away, these effects again become more significant. In Zone 7, there is a difference of over 40% between the two models. This being said, as the steady-state concentration is lower at a higher air change rate, as we can see from Fig. 2(d), the quanta concentration value in this zone is very small compared to all other cases.

These results demonstrate that when using these models in complex multi-zone environments, there will still likely be zones or time periods for which a steady-state assumption gives an overestimation. Although in terms of a risk assessment this potentially errs on the side of caution, it can also lead to underestimates in quantifying outbreaks. If the zonal flows are not considered, as shown in Noakes and Sleigh [17], it can result in a significant underestimation of infectious quanta emission where models are used to "back calculate" from an outbreak. Although not explicitly demonstrated here, the converse would also be true. Once an infectious person has left a space, the steady-state model returns immediately to zero, which would therefore underestimate the transient model, failing to capture the decay curve that would be experienced in reality.

The consequences of the overestimation of the transient quanta concentration solution translates into the expected cumulative exposures over time. Fig. 4, shows the solution for the exposures compartment of the SE model for four different ventilation rates in terms of total exposures across all susceptible people within the respiratory ward rather than in each zone. This illustrates the overall difference between using the steady-state concentration model versus the transient model and how this affects the number of estimated exposures, which again is being overestimated when using the solution from the steady-state concentration.

When considering lower ventilation rates, as previously done in Figs. 2(b) and 2(a) where the overestimation for the concentration is higher, this consequently translates into a larger difference between the estimated exposures compartmental model when using the steady-state concentration versus the transient (Figs. 4(b) and 4(a)). It is also worth highlighting the increase in the overall quanta concentration in each space and thus an increased number of exposures. Despite this being an expected consequence, it illustrates the effects that ventilation has on an outbreak, reducing the overall risk of transmission.

As expected, at the recommended ventilation rate of 6 ACH (Fig. 4(d)), there is very little difference between the predictions for the number of exposed individuals and that after the 4 h period, not even 1
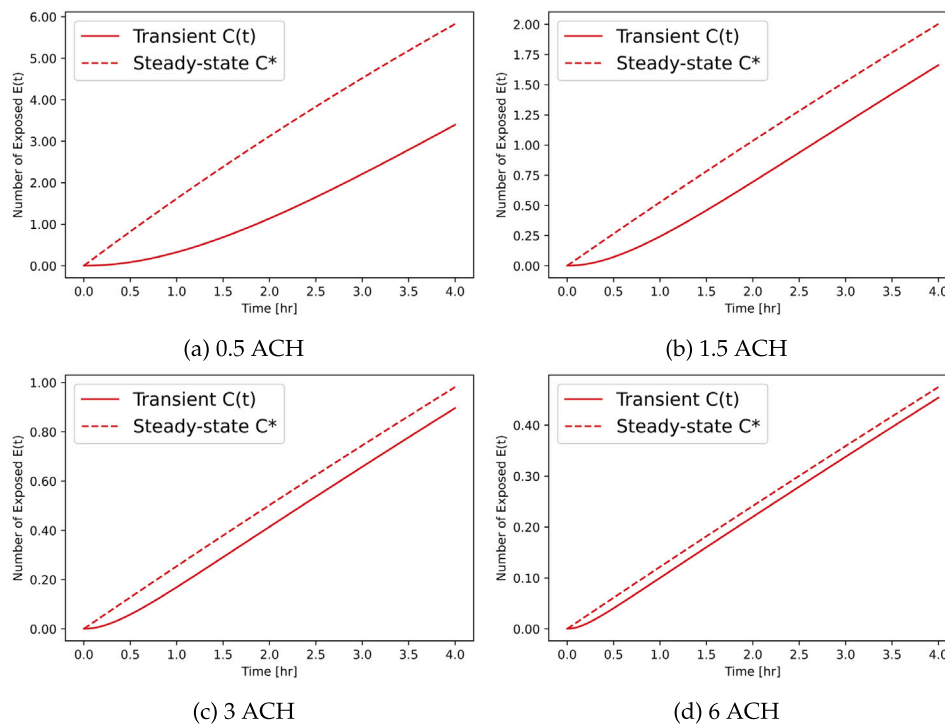
(a) 0.5 ACH   (b) 1.5 ACH

(c) 3 ACH   (d) 6 ACH

Fig. 4. The solution for the exposed compartmental model using the transient solution for concentration of pathogen in the air (solid) and the steady-state solution (dashed) for various ventilation rates for the fixed infector case.
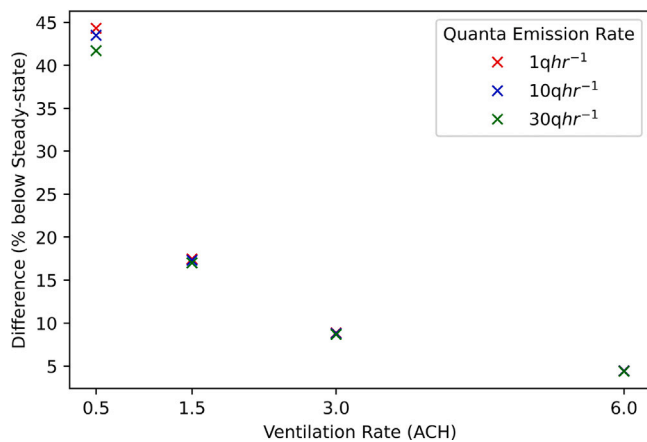

Fig. 5. The relative difference between the predicted exposures from the epidemic model, calculated as $\frac{E^* - E(t=4\,\mathrm{h})}{E^*}$ x 100, using the steady-state and the transient solution for concentration of airborne pathogen for 3 different quanta emission rates across 4 different ventilation settings for the fixed infector case.

exposure is predicted. This highlights the benefits of good ventilation within spaces when trying to reduce transmission.

3.1.3. Varying the quanta emission rate

Fig. 5 explores the relative difference between the cumulative number of exposed individuals by time $t = 4$ h plotted against increasing ventilation rate, when using the steady-state concentration solution versus the transient solution for varying quanta emission rates.

As seen previously in the concentration data in Fig. 3, overestimation using the steady-state model is also seen in the exposures. This decreases as the ventilation rate increases with a difference of more than 40% in predicted exposures between the two models with a ventilation rate of 0.5 ACH compared to around 10% when the ventilation rate is 3 ACH. The results also show a small effect of the

quanta emission rate, with the greatest difference at low ventilation rates; as the ventilation rate increases to 3 ACH and beyond there is negligible difference between the two models for different emission rates. At 6 ACH the relative difference between the two models is < 5% regardless of the infectiousness of an individual, again suggesting that the recommended ventilation rates for hospital wards in the UK likely eliminate the need for consideration of transient effects, except for very short duration events, regardless of the quanta emission rate. However, in scenarios with poor ventilation, it is possible to experience different accuracy when using steady-state versus the transient assumptions and it is important to consider the infectiousness of an infector. Results for the concentration solution, exposure solution and the relative difference between the steady-state solutions and transient solutions, illustrate that ventilation rates in a scenario are the main driving factor which are likely to determine the outcome of an airborne outbreak and also whether a transient or the steady-state approximation is most appropriate.

3.2. Case study 2: Transient infectious HCW

3.2.1. A real respiratory ward

In this second case, a different, more realistic geometry was used. Floor plans were obtained from a UK NHS Hospital Trust Respiratory Ward, from which a 12-zone geometry subset was chosen. This subset consisted of a ward layout containing patient single and multi-bed wards, HCW and treatment room environments. The geometry (Fig. 6) is used for the simulations with a transient infector where: Zones 1 and 2 represent 4-bed bays (with 4 susceptible people in each); Zones 3 and 4 represent single rooms (with 1 susceptible person in each); Zone 5 is the nursing station (with 4 susceptible people and 1 initial infector); Zone 6 is a connecting corridor split into 3 zones, namely Zone 6a, 6b, and 6c (with 4 susceptible people in total, representing staff); and Zones 7–10 are clinical treatment rooms (with 6 susceptible people across these zones - 3 in Zone 8, 2 in Zone 9 and 1 in Zone 10). There are a total of 24 fixed susceptible people, with 1 infector who is allowed to move through the space following a pre-defined
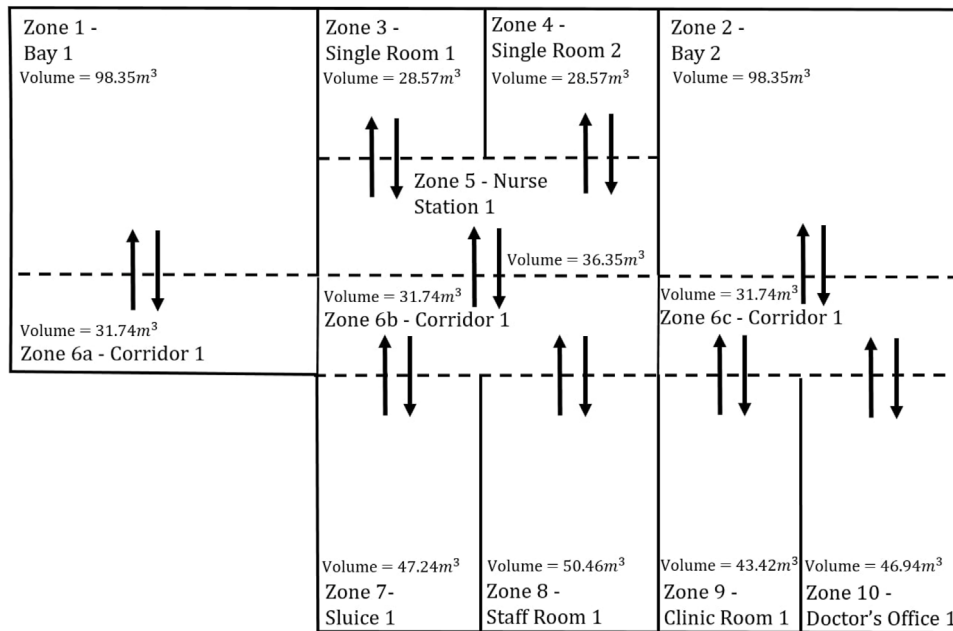
Fig. 6. Illustration of the selected geometry, a 12-zone subset of a UK Respiratory Ward showing the zone number, type and volume for each zone.

Table 1
Frequency of HCW visits to patients for chosen zones on a UK Respiratory Ward for a typical 24 h period.

Bed	Observations	Drug round	Doctor/ Medical review	Total Visits
Bay 1 - Bed 1	7	4	1	12
Bay 1 - Bed 2	8	4	1	13
Bay 1 - Bed 4	8	4	1	13
Single Room 1	4	3	1	8
Single Room 2	7	4	1	12

schedule. This gives initial conditions for the epidemic model as $S_0 = (4, 4, 1, 1, 4, 1, 2, 1, 0, 3, 2, 1)$, $E_0 = 0$ for each zone, and $I_0 = 1$ in Zone 5 only, and is zero for all other zones. The transient infector moves from one zone to another in time, but once they are in a particular zone we do not consider interaction with specific patients and focus on modelling the airborne concentration and exposure in the whole zone.

In order to allow the infector to move around the space, it was necessary to have a realistic schedule. Information provided by a senior clinician on the typical number of times a HCW visited a patient was used to define typical activities as shown in Table 1.

From Table 1, an average of the number of visits to a bed per day is 11.6 per 24 h period. Taking this as ≈ 12 per day, it was assumed that $\frac{1}{3}$ of the visits were at night and $\frac{2}{3}$ of the visits during a 12 h day time period. This gave an estimate of 8 visits throughout a 12 h day time period which is approximately one visit every 90 min to each bed. Working on the basis that across two 4-bed bays and two single rooms there are 10 beds in total from the chosen geometry (Fig. 6), this gives an approximate time of 9 min per visit per bed. For a 4-bed bay it was assumed that approximately 35 min were spent on each at one time, and a single bed room taken as 10 min per round. This then leads to the following schedule:

1. Infectious HCW sets up at nurse station for 30 min — Zone 5
2. Infectious HCW visits Bay 1 to complete round lasting 35 min — Zone 1
3. Infectious HCW visits Bay 2 to complete round lasting 35 min — Zone 2
4. Infectious HCW visits Single Room 1 to complete round lasting 10 min — Zone 3

5. Infectious HCW visits Single Room 2 to complete round lasting 10 min — Zone 4

This schedule lasts for 2 h, which is then repeated creating a 4 h simulation, with 2 visits to each bed within the period of modelling. Movements such as between zones through corridors have been ignored and assumed to be sufficiently short in duration to have no significant effect.

A CONTAM model of the airflow was used to obtain realistic inter-zonal flow rates, β_{kj}, following the methodology in Section 2.2. The CONTAM set-up in Fig. 7 shows the location of airflow openings with an arrow illustrating the positive airflow direction. Table 2 shows the corresponding description to each of the openings. The building orientation, windows, and doors were used to determine ward inter-zonal flows for three steady-state ventilation rates, 0.5 ACH, 1.5 ACH and 3 ACH. The CONTAM model included the effect of the infectious HCW schedule on the inter-zonal flows, with doors opened as appropriate for 1 minute to simulate the HCW entering a zone. The inter-zonal flow rates were then used in the transport equation for multi-zone concentration of airborne pathogen (Eq. (4)) as discussed in Section 2.2. As previously, the quanta emission rate of infectious individuals is taken to be $q_k = 0.5$ quanta min^{-1}, $\forall k$ [17] and the pulmonary rate of all individuals is taken to be $p_k = 0.01$ m^3 min^{-1}, $\forall k$. The initial concentration is taken to be $C_0 = 0$ in each zone.

3.2.2. Effect of ventilation rate

Fig. 8 shows solutions for the transient concentration of airborne quanta for three ventilation rates, alongside the steady-state solution. For clarity, only the solution for the 5 zones in which the infector visits have been included on this plot. Due to the transient infector moving through the zones at different time periods we can observe different dynamics to the concentration solutions seen in the fixed infector case as in Fig. 2.

The overestimation by the steady-state approximation is still present, but is much more varied than when the infectious individual is at a fixed location. For example, when the infectious person is in Zone 1, the transient quanta concentration almost reaches the steady-state value by the time the infectious person leaves, whereas in Zone 3, the peak transient concentration is less than half of the steady-state value.

Unlike the steady-state approximation which immediately returns to zero concentration when the infectious person leaves, the transient

Table 2

Airflow element descriptions, corresponding element number in Fig. 7, and the boundary condition defined within CONTAM model for the 12-zone respiratory ward.

| Elements	Number	CONTAM Airflow Type
Top-hinged Window	1,4,7,10,34,37,40,43	Two-way Flow/Two-opening
Sash Window	2,5,8,11,35,38,41,44	Two-way Flow/Two-opening
Double Door	13,15,17,20	Two-way Flow/Two-opening
Single Door	26,28,30,32	Two-way Flow/Two-opening
Under-door Gap	14,16,18,21,27,29,31,33	Two-way Flow/Two-opening
Leakage	3,6,9,12,36,39,42,45	One-way Flow Using Powerlaw/Crack Description
Corridor End	22,25	One-way Flow Using Powerlaw/Orifice Area Data
Corridor (Long)	19,23,24	Two-way Flow/Two-opening
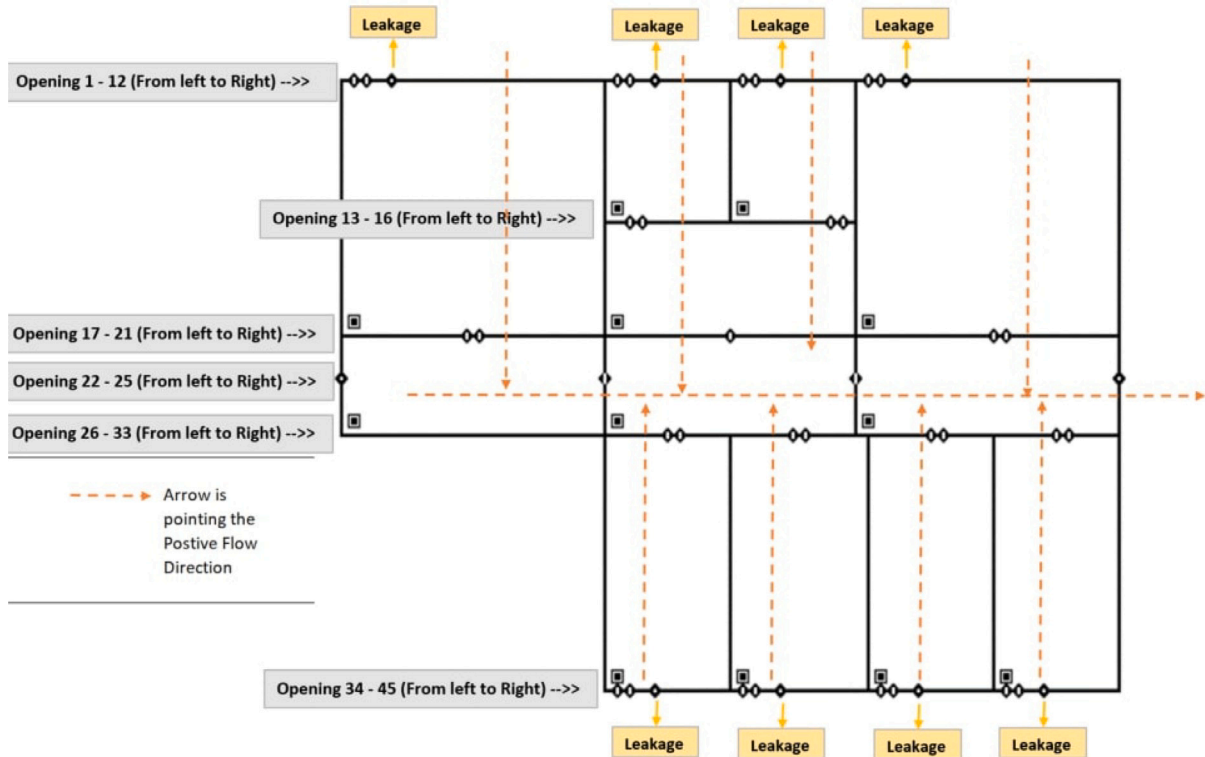
Fig. 7. CONTAM model set-up, illustrating the geometry, airflow elements (small diamonds) and corresponding number (opening numbers on the left of the figure) and the arrow illustrating the direction taken as positive for the airflow. The corresponding airflow element type to each number can be seen in Table 2. The square icon in each zone contains the zonal set-up.

model captures the dilution rate of the quanta in the air over time. The time period for this dilution depends on ventilation rate, and for lower ventilation rates its possible to see that the concentration never returns to zero. By the time the infectious person returns for the second ward visit, the quanta concentration is compounded and thus, upon leaving for the second time the airborne concentration is higher than after the first visit.

A similar effect can also be seen with zones where the infectious person is not present, but are linked through airflow to the zone where the infectious person is. Here, we see an opposite effect where the concentration of pathogen is non-zero and begins to increase despite the absence of an infector. This is due to the effects of mixing, ventilation and inter-zonal airflow. The steady-state model fails to capture this gradual increase in other zones. It does model a non-zero concentration in connected zones but these are small, and the presence of an infector dominates.

Fig. 9 shows the relative difference between the steady-state and transient models for Zone 5 (the nurse station), and Zone 3 (a single-bed room) for the concentration of pathogen solution. By using these two different zones, we allow for a different volume room in each case

and a different length of visit by the infectious person. In both cases, the relative difference has been calculated at the end of the first visit and at the end of the second visit to explore the effects of compounding and dilution due to the movement of the transient infector and inter-zonal flow connections in a multi-zone system.

Zone 5 (Nurse Station) has a smaller relative difference between models and is therefore better approximated by the steady-state than Zone 3 (single-bed room). The difference between the two rooms increases with the ventilation rate. However, the infectious person spends only 10 min in the single room, as opposed to 30 min in the nurse station which is also likely to be a major contributor to the difference between the two models. The longer the infectious person stays in a zone, the closer the quanta concentration will get to the steady-state value; since we are focusing on relative difference, the zone with the infectious person present for the longest time will have a smaller relative difference between the two models. As previously, the higher ventilation rate, the better the approximation by the steady-state model regardless of the time spent in the zone, and we see this for both zones. Other factors such as volume and time can also increase the effects of ventilation on the accuracy of the steady-state approximation for
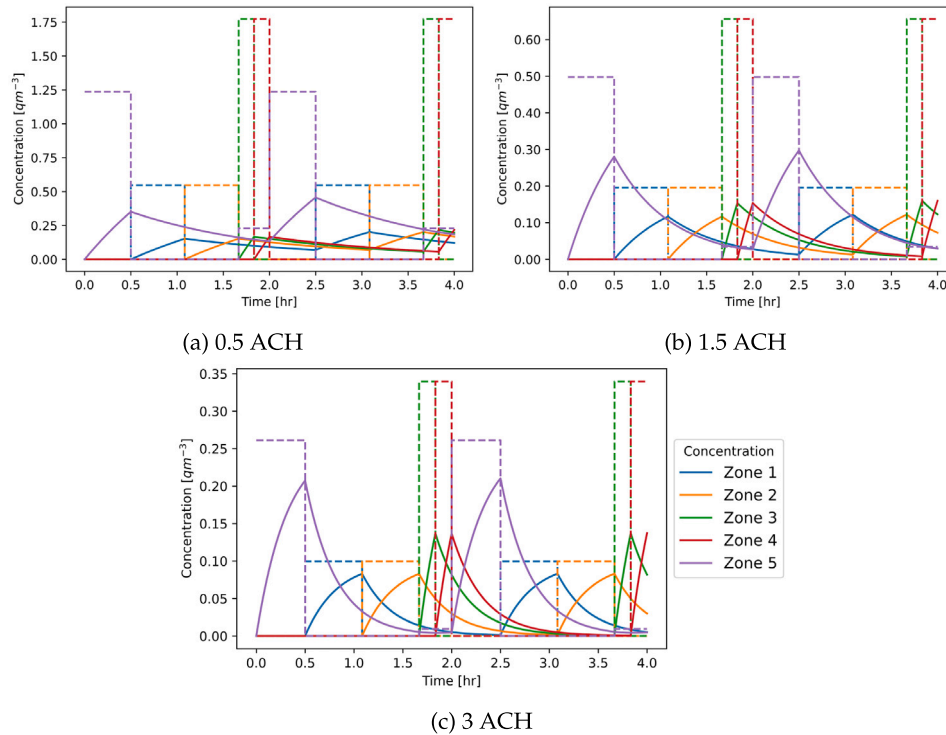
(a) 0.5 ACH

(b) 1.5 ACH

(c) 3 ACH

Fig. 8. Modelled concentration of pathogen in the air for the transient solution (solid) and the steady-state solution (dashed) for three ventilation rates for the transient infector case.
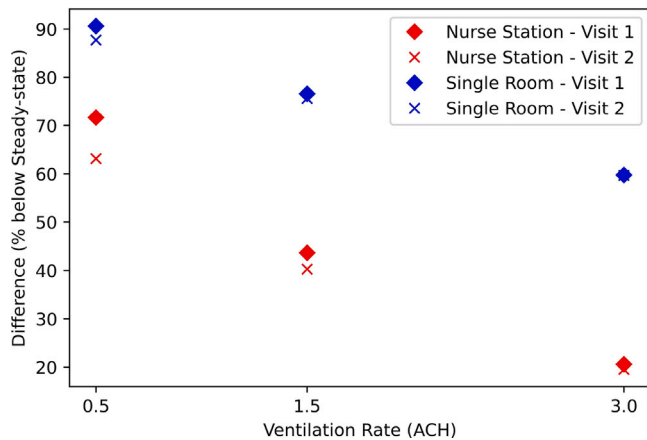

Fig. 9. The relative difference between the concentration values of the steady-state and the transient solution, calculated as $\frac{C^* - C(t)}{C^*}$ x 100, for Zone 5 (the Nurse station), and Zone 3 (a single-bed room) after the first and last visit with 3 different ventilation settings for the transient infector case.

a particular zone. For example, in the single room, upon increasing the ventilation rate from 0.5 ACH to 3 ACH, the steady-state model is around 30% more accurate, where as in the case of the slightly bigger volume and longer visitation of the nurse station, this increase is closer to around 50%.

As previously mentioned, there is evidence that other zones are affected by the infectious air transported from connecting zones when the infector is not necessarily present, or that the transient model describes a decaying airborne concentration when the infectious individual leaves a zone. This can be illustrated by focusing on each zone in turn in Fig. 9. When comparing the relative difference at the end of the first ward visit compared to the second visit, at higher ventilation rates the steady-state approximation for the first and second visit is very

similar. However, at the lowest ventilation rate, the overestimation by the steady-state model decreases from the first visit to the second. This demonstrates the uncertainty of a steady-state model for approximating transient multi-zone environments. For scenarios with low or varying ventilation in multi-zone spaces of varying geometry, it would be difficult to characterise the accuracy of the steady-state approximation due the added transient effects from the infectious person moving around the space. This difference is eliminated with increasing ventilation rate, where the steady-state approximation not only becomes better, but there is little difference between each visit during the simulated time period. This analysis demonstrates the added complexity that is introduced by an infectious person moving around a space which is ubiquitous in real-life scenarios, and how the transient model is able to capture this with greater consistency.

In a similar way to case one, any overestimation experienced through using a steady-state model for the concentration of pathogen instead of the more accurate transient version leads to an overestimation in the predicted number of exposures as well. This is illustrated in Fig. 10, showing the solution for both steady-state and transient models of the exposed compartment of the SE model for three different ventilation rates.

These results show that the differences between steady-state and transient model concentrations are translated into the risks predicted through the epidemic model. This follows the same pattern observed in the fixed infector case with the steady-state model overestimation becoming greater as the ventilation rate decreases. Another notable feature in Fig. 10 is the variation as the transient infector moves around. Unlike the case with the fixed infector, the periods where the infector moves are reflected with varying overestimation at each period. For example in the first 30 min in Fig. 10(b), it is possible to observe the steady-state solution begin to look like it could diverge from the transient model as opposed to being a linear overestimation. This gives motivation for further analysis into a zonal level analysis rather than on a population level. For example, by looking into the effects of extending the period of time when an infectious person is present during a drug round.
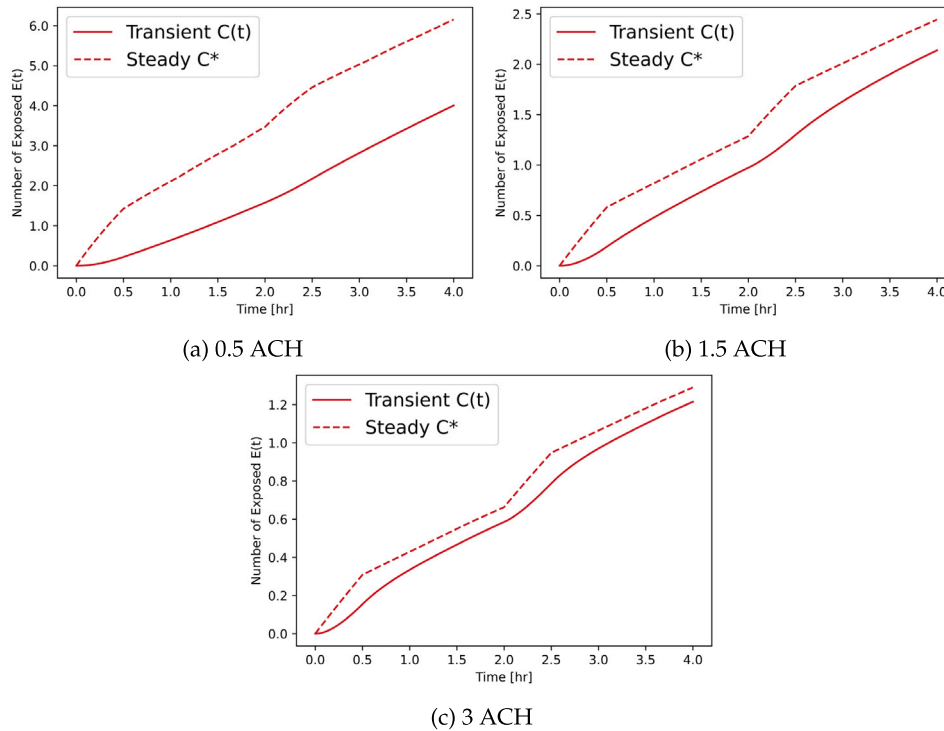
(a) 0.5 ACH

(b) 1.5 ACH

(c) 3 ACH

Fig. 10. The solution for the exposed compartmental model using the transient solution for quanta concentration in the air (solid) and the steady-state solution (dashed) for three ventilation rates for the transient infector case.
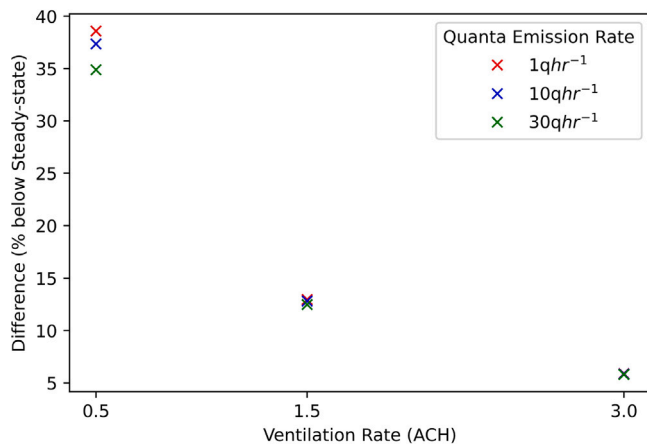

Fig. 11. The relative difference between the predicted exposures from the epidemic model, calculated as $\frac{E^* - E(t=4\,h)}{E^*}$ x 100, using the steady-state and the transient solution for concentration of airborne pathogen for 3 different Quanta emission rates across 3 different ventilation settings for the transient infector case.

The effects of the ventilation rate on the overall number of exposures can also be seen in Fig. 10. As in the fixed infector case, increasing the ventilation rate reduces the quanta concentration in each zone and thus, potentially the total number of exposures in an outbreak.

3.2.3. Varying quanta rates

In Fig. 11, the relative difference of the final exposed value ($t = 4$ h) from the exposed compartment of the SE model can be seen for three ventilation rates, and for three different quanta production rates.

A very similar outcome to the fixed infector case can be seen. The difference between models decreases as the ventilation rate is increased, and the relative difference for each quanta production rates align; for the well ventilated case, all three quanta production rates

display an almost identical overestimation when using a steady-state approximation. Despite having a transient infector moving around the space, the model accuracy is similar when predicting exposures whether using a transient or steady-state concentration model. Given that the transient infector case uses more realistic inter-zonal flow values than in the fixed infector model, a greater difference in the two results may have been expected. This provides motivation for further analysis into the inter-zonal flows and mixing rates, and the possible effects these could have on the outbreak dynamics.

4. Conclusion

Through extension of a transport equation for the concentration of airborne pathogen to a multi-zonal environment and its coupling with an Susceptible–Exposed epidemic model, we have demonstrated the ability to analyse the potential importance of transient effects on outbreaks in multi-zone indoor spaces. By considering a transient solution describing the multi-zone concentration, rather than the more commonly applied steady-state Wells–Riley model, we are able to better predict the likely quanta concentration in indoor spaces and how this may effect the transport of airborne pathogens to neighbouring spaces. Through various occupancy, ventilation and quanta emission scenarios, a comparison of the two models has shown the importance of considering transient effects and the ability of the transient model to capture some of the complexities experienced when attempting to model real-life scenarios. Additionally, even when considering the transient solution, the numerical model has a computational time of 1.23 s for the fixed infector case, and 1.59 s for the transient infector. Given that this includes the steady-state model calculation and comparison as well, it demonstrates no computational benefit in using the steady-state model in place of the transient model for these scenarios. This consequently leads to a better prediction of exposures during an outbreak, and thus, the potential for better implementation of mitigation strategies and resources to situations which would benefit the most.

It is important to highlight that the steady-state model may result in a "worst-case" style of analysis which may be applicable and even

favourable in certain scenarios. Using the steady-state approach when planning interventions such as ventilation design can result in a "safety factor" to provide resilience in design. It is also likely to be appropriate for longer time period scenarios where the infector can be assumed to be fixed in one location, although the zonal variation in concentration still needs to be considered. However, when this is applied to short timescale events, and a moving infector, the differences between the models are significant. In using such models to inform management or temporary environmental interventions in a hospital setting where resources are often scarce and bed occupancy is high [40], it is important that methods can offer efficient and realistic assessments to pragmatically deploy resources. Using a transient approach can allow for a more realistic representation complex scenarios but the model presented is also versatile and adaptable, making it suitable for many outbreak scenarios and disease settings.

With the use of ventilation rates between 0.5 and 6 ACH, we have shown the benefit of increased ventilation rates on various scenarios. Increasing the ventilation rate leads to an overall reduction in the total quanta concentration in a given space and the consequent number of exposures resulting from an infector. At higher ventilation rates, there is less variability between the model predictions, with the expected exposures in an environment less dependent on the choice of parameters in models. It is also worth noting that despite the variation in ventilation rates through the models, the inter-zonal flow rates remained fixed for each scenario. This assumption may not hold in reality, and the inter-zonal flow rates would most likely change alongside the ventilation rates, which is something that should be considered in future work.

One of the main limitations of a study such as this is validation. Although we have explored sensitivity to ventilation rates, emission rates and the behaviour of an infector, the work presented in this study is based on a model calculation. Previous work has shown that the Wells–Riley model can match transmission rates observed in large outbreaks [20]. There is also evidence of airborne transmission between neighbouring spaces including for COVID-19 in quarantine hotels [41] and hospital wards [42]. Airflow models such as CONTAM have also had prior validation [43], and initial comparison between the CONTAM model of our respiratory ward and CO2 measurements in the ward suggest that the airflows used in this paper are realistic. Although it is clear that this work would benefit from observational validation of an outbreak, this is extremely difficult in complex multi-zone settings in a busy hospital ward. In practice, it is almost impossible to identify exactly where an infection originated and the direct and indirect contacts of an infector, especially when considering long range exposure in a hospital environment. Exposure is complicated by multiple shift patterns, staff changes, movement within and between rooms, multiple zones and identifying whether the infection was airborne or contracted via an alternative route such as fomite transmission. The models in the current paper also only consider the far-field airborne exposure, and do not include the potential for exposure to higher concentrations of aerosols and droplets when an infector has close range interaction with a susceptible. In the future, this work could explore validation and close range exposures via a CFD study, but this would likely be limited to a single room split into multiple zones as a multi-zone ward geometry such as the one used here would be impractical and computationally expensive to replicate over an extended time period.

Despite the successful demonstration of the transient model, it is likely that there are certain scenarios where a steady-state approximation would be sufficient. However, we have demonstrated that these need careful consideration, with the duration of time the infector spends in the room, the ventilation rate and the inter-zonal flows all affecting whether the model is appropriate. Our further work will apply these models to a much broader set of scenarios exploring further the effects of variable ventilation rates with weather and season, inter-zonal flows and mixing, and occupancy behaviours. However, through this approach, the ability to better represent more realistic scenarios has been illustrated and future work on specific outbreak scenarios will hopefully establish its value further.

Ethical approval

This study does not contain any studies with human or animal subjects performed by any of the authors.

CRediT authorship contribution statement

Alexander J. Edwards: Writing – review & editing, Writing – original draft, Visualization, Validation, Software, Resources, Project administration, Methodology, Investigation, Funding acquisition, Formal analysis, Data curation, Conceptualization. **Lee Benson:** Software. **Zeyu Guo:** Methodology. **Martín López-García:** Writing – review & editing, Writing – original draft, Conceptualization. **Catherine J. Noakes:** Writing – review & editing, Writing – original draft, Conceptualization. **Daniel Peckham:** Writing – review & editing, Writing – original draft, Conceptualization. **Marco-Felipe King:** Writing – review & editing, Writing – original draft, Conceptualization.

Declaration of competing interest

The authors declare that they have no known competing financial interests or personal relationships that could have appeared to influence the work reported in this paper.

Data availability

The code and data is available at https://github.com/scaje/Multi-zone_Hospital_conc_AJE.git.

Acknowledgements

References

[1] C.C. Wang, K.A. Prather, J. Sznitman, J.L. Jimenez, S.S. Lakdawala, Z. Tufekci, L.C. Marr, Airborne transmission of respiratory viruses, Science 373 (6558) (2021) eabd9149, http://dx.doi.org/10.1126/science.abd9149, URL https://www.science.org/doi/abs/10.1126/science.abd9149.

[2] NHS, NHS England Respiratory Disease, 2022, https://www.england.nhs.uk/ourwork/clinical-policy/respiratory-disease/ (Accessed: 07/09/2021).

[3] L. Bourouiba, Turbulent gas clouds and respiratory pathogen emissions: Potential implications for reducing transmission of COVID-19, JAMA (ISSN: 0098-7484) 323 (18) (2020) 1837–1838, http://dx.doi.org/10.1001/jama.2020.4756.

[4] K.P. Fennelly, Particle sizes of infectious aerosols: implications for infection control, The Lancet Respir. Med. (ISSN: 2213-2600) 8 (9) (2020) 914–924, http://dx.doi.org/10.1016/S2213-2600(20)30323-4, URL https://www.sciencedirect.com/science/article/pii/S2213260020303234.

[5] G. Buonanno, L. Stabile, L. Morawska, Estimation of airborne viral emission: Quanta emission rate of SARS-CoV-2 for infection risk assessment, Environ. Int. 141 (2020) 105794.

[6] W. Hiwar, H. Kharrufa, M. King, N. Salman, L. Fletcher, C. Noakes, Multiplate air passive sampler to measure deposition rate of airborne microorganisms over time, in: Proceedings of the 16th Conference of the International Society of Indoor Air Quality and Climate: Creative and Smart Solutions for Better Built Environments, Indoor Air 2020, 1, International Society of Indoor Air Quality and Climate (ISIAQ), 2021, pp. 708–713.

[7] T.G. Foat, B. Higgins, C. Abbs, T. Maishman, S. Coldrick, A. Kelsey, M.J. Ivings, S.T. Parker, C.J. Noakes, Modeling the effect of temperature and relative humidity on exposure to SARS-CoV-2 in a mechanically ventilated room, Indoor Air 32 (11) (2022) e13146, http://dx.doi.org/10.1111/ina.13146, URL https://onlinelibrary.wiley.com/doi/abs/10.1111/ina.13146 e13146 INA-22-08-402.R1.

[8] M. Jayaweera, H. Perera, B. Gunawardana, J. Manatunge, Transmission of COVID-19 virus by droplets and aerosols: A critical review on the unresolved dichotomy, Environ. Res. 188 (2020) 109819.

[9] H. Qian, Y. Li, P.V. Nielsen, X. Huang, Spatial distribution of infection risk of SARS transmission in a hospital ward, Build. Environ. 44 (8) (2009) 1651–1658.

[10] M.-F. King, C. Noakes, P. Sleigh, M. Camargo-Valero, Bioaerosol deposition in single and two-bed hospital rooms: A numerical and experimental study, Build. Environ. 59 (2013) 436–447.

[11] C.H. Cheong, S. Lee, Case study of airborne pathogen dispersion patterns in emergency departments with different ventilation and partition conditions, Int. J. Environ. Res. Public Health 15 (3) (2018) 510.

[12] C.J. Noakes, C.B. Beggs, P.A. Sleigh, K.G. Kerr, Modelling the transmission of airborne infections in enclosed spaces, Epidemiol. Infect. (ISSN: 09502688) 134 (5) (2006) 1082–1091, http://dx.doi.org/10.1017/S0950268806005875.

[13] S. Robertson, S.D. Lawn, A. Welte, L.-G. Bekker, R. Wood, Tuberculosis in a South African prison–a transmission modelling analysis, South African Medical Journal 101 (11) (2011) 809–813.

[14] W.F. Wells, et al., Airborne contagion and air hygiene. An ecological study of droplet infections, 1955.

[15] E. Riley, G. Murphy, R. Riley, Airborne spread of measles in a suburban elementary school, Am. J. Epidemiol. 107 (5) (1978) 421–432.

[16] C. Zemouri, S. Awad, C. Volgenant, W. Crielaard, A. Laheij, J. De Soet, Modeling of the transmission of coronaviruses, measles virus, influenza virus, Mycobacterium tuberculosis, and Legionella pneumophila in dental clinics, J. Dent. Res. 99 (10) (2020) 1192–1198.

[17] C.J. Noakes, P.A. Sleigh, Mathematical models for assessing the role of airflow on the risk of airborne infection in hospital wards, J. R. Soc. Interface (ISSN: 17425662) 6 (2009) http://dx.doi.org/10.1098/rsif.2009.0305.focus.

[18] P.J. Bueno de Mesquita, C.J. Noakes, D.K. Milton, Quantitative aerobiologic analysis of an influenza human challenge-transmission trial, Indoor Air 30 (6) (2020) 1189–1198, http://dx.doi.org/10.1111/ina.12701, URL https://onlinelibrary.wiley.com/doi/abs/10.1111/ina.12701.

[19] A. Mikszewski, L. Stabile, G. Buonanno, L. Morawska, The airborne contagiousness of respiratory viruses: a comparative analysis and implications for mitigation, Geosci. Front. (2021) 101285.

[20] Z. Peng, A.P. Rojas, E. Kropff, W. Bahnfleth, G. Buonanno, S.J. Dancer, J. Kurnitski, Y. Li, M.G. Loomans, L.C. Marr, et al., Practical indicators for risk of airborne transmission in shared indoor environments and their application to COVID-19 outbreaks, Environ. Sci. Technol. 56 (2) (2022) 1125–1137.

[21] S. Rudnick, D. Milton, Risk of indoor airborne infection transmission estimated from carbon dioxide concentration, Indoor Air 13 (3) (2003) 237–245.

[22] C. Vouriot, H. Burridge, C. Noakes, P. Linden, Seasonal variation in airborne infection risk in schools due to changes in ventilation inferred from monitored carbon dioxide, Indoor Air 31 (4) (2021) 1154–1163.

[23] Y. Guo, H. Qian, Z. Sun, J. Cao, F. Liu, X. Luo, R. Ling, L.B. Weschler, J. Mo, Y. Zhang, Assessing and controlling infection risk with Wells-Riley model and spatial flow impact factor (SFIF), Sustainable Cities Soc. 67 (2021) 102719.

[24] M. López-García, M.F. King, C.J. Noakes, A Multicompartment SIS Stochastic Model with Zonal Ventilation for the Spread of Nosocomial Infections: Detection, Outbreak Management, and Infection Control, Risk Anal. (ISSN: 15396924) 39 (8) (2019) 1825–1842, http://dx.doi.org/10.1111/risa.13300.

[25] NIST, NIST CONTAM, 2022, https://www.nist.gov/services-resources/software/contam (Accessed: 17/05/2022).

[26] Z. Liu, Q. Liang, H. Liao, W. Yang, C. Lu, Effects of short-term and long-term exposure to ambient air pollution and temperature on long recovery duration in COVID-19 patients, Environ. Res. 216 (2023) 114781.

[27] S. Yan, L.L. Wang, M.J. Birnkrant, J. Zhai, S.L. Miller, Evaluating SARS-CoV-2 airborne quanta transmission and exposure risk in a mechanically ventilated multizone office building, Build. Environ. (2022) 109184.

[28] C.H. Cheong, B. Park, S. Lee, Design method to prevent airborne infection in an emergency department, J. Asian Archit. Build. Eng. 17 (3) (2018) 581–588.

[29] P. Shrestha, J.W. DeGraw, M. Zhang, X. Liu, Multizonal modeling of SARS-CoV-2 aerosol dispersion in a virtual office building, Build. Environ. 206 (2021) 108347.

[30] S. Parker, C. Coffey, J. Gravesen, J. Kirkpatrick, K. Ratcliffe, B. Lingard, J. Nally, Contaminant ingress into multizone buildings: An analytical state-space approach, in: Building Simulation, 7, Springer, 2014, pp. 57–71.

[31] W.O. Kermack, A.G. McKendrick, A contribution to the mathematical theory of epidemics, Proc. R. Soc. Lond. Ser. A, Containing Papers of A Mathematical and Physical Character 115 (772) (1927) 700–721.

[32] J. Arino, C. Sun, W. Yang, Revisiting a two-patch SIS model with infection during transport, Math. Med. Biol.: A Journal of the IMA 33 (1) (2016) 29–55.

[33] C. Sun, Y.-H. Hsieh, Global analysis of an SEIR model with varying population size and vaccination, Appl. Math. Model. 34 (10) (2010) 2685–2697.

[34] D. Miller, M.-F. King, J. Nally, J.R. Drodge, G.I. Reeves, A.M. Bate, H. Cooper, U. Dalrymple, I. Hall, M. López-García, et al., Modeling the factors that influence exposure to SARS-CoV-2 on a subway train carriage, Indoor Air (2022) e12976.

[35] W. Dols, B. Polidoro, CONTAM user guide and program documentation version 3.2, 2015, http://dx.doi.org/10.6028/NIST.TN.1887.

[36] B. Polidoro, L.C. Ng, W.S. Dols, et al., CONTAM results export tool, Technical Note-1912, Gaithersburg, MD: National Institute of Standards and Technology, 2016.

[37] NIST, Results Export Tool, 2022, https://pages.nist.gov/CONTAM-apps/webapps/contam_results_exporter/index.htm (Accessed: 22/10/2022).

[38] G. Guyot, S. Sayah, S. Guernouti, A. Mélois, Role of ventilation on the transmission of viruses in buildings, from a single zone to a multizone approach, Indoor Air 32 (8) (2022) e13097.

[39] N.H.S. England, HTM03-01 Specialised Ventilation for Healthcare Buildings, 2021, URL https://www.england.nhs.uk/publication/specialised-ventilation-for-healthcare-buildings/.

[40] A. Dowd, Hospital bed occupancy rates in England reach dangerously high levels, BMJ 374 (2021) http://dx.doi.org/10.1136/bmj.n2079, URL https://www.bmj.com/content/374/bmj.n2079.

[41] SAGE, EMG/Transmission group/SPI-B: COVID-19 transmission in hotels and managed quarantine facilities (MQFs), 2021, https://www.gov.uk/government/publications/emg-covid-19-transmission-in-hotels-and-managed-quarantine-facilities-mqfs-9-september-2021.

[42] J. Jung, J. Lee, S. Jo, S. Bae, J.Y. Kim, H.H. Cha, J.Y. Lim, S.H. Kwak, M.J. Hong, et al., Nosocomial outbreak of COVID-19 in a hematologic ward, Infection & Cheomotherapy 53 (2) (2021) 332–341.

[43] F. Haghighat, A.C. Megri, A comprehensive validation of two airflow models—COMIS and CONTAM, Indoor Air 6 (4) (1996) 278–288, http://dx.doi.org/10.1111/j.1600-0668.1996.00007.x, URL https://onlinelibrary.wiley.com/doi/abs/10.1111/j.1600-0668.1996.00007.x.